AIMS Mathematics, 11(11): 39645–39669.
DOI: 10.3934/math.20261527
Received: 30 August 2026
Revised: 08 November 2026
Accepted: 13 November 2026
Published: 26 November 2026

https://www.aimspress.com/journal/Math

Research article

Influence of gravity fields on a photomagnetothermoelastic model for hydromechanical wave propagation in a poro-semiconductor medium

Kawther K. Alarfaj[1,*], **Maryam Khalid Alarfaj**[2] **and Doaa M. Salah**[3]

[1] Department of Mathematics and Statistics, College of Science, King Faisal University, P.O. Box 400, Al-Ahsa 31982, Saudi Arabia

[2] Computer and Information Technology, Applied College, King Faisal University, P.O. Box 400, Al-Ahsa 31982, Saudi Arabia

[3] Department of Mathematics, Faculty of Science, Sohag, Sohag University, Egypt

* **Correspondence:** Email: kkarfaj@kfu.edu.sa.

Abstract: The formulation of a coupled thermohydromechanical photoelastic model is presented for time-dependent wave propagation in a fluid-saturated, porous, semiconducting half-space under the influence of electromagnetic, magnetic, and gravity fields. Governing equations which involve generalized thermoelasticity, hydromechanics, and photoelasticity are solved by means of normal mode analysis with computation in Mathematica for two-dimensional wave propagation. The influences of time, permittivity (ϵ_0), magnetic field strength, and gravity on temperature, carrier density, pore-fluid pressure, acoustic pressure, displacement, and stress have been investigated. It has been found that the electromagnetic and magnetic fields primarily influence carrier density and stress, whereas gravity significantly influences pore-fluid pressure and thermal gradients. Temporal behavior sheds light on dynamic coupling and energy transfer between the fields. The theory enriches the classical theory of poroelasticity and provides a physical insight into the problem of wave propagation and stress generation in porous semiconductors. This present model is an extension of many existing formulations of thermoelastic and photothermal semiconductors. This study reveals novel aspects of coupled wave propagation in thermohydroelectromagnetics. The results of this study are significant for the design and optimization of porous semiconductors working in laser exposure and magnetic conditions.

Keywords: photoelastic wave propagation; poro-semiconductor; electromagnetic field; gravity effects; normal mode analysis
Mathematics Subject Classification: 26D15, 26E60, 26A33, 60E05, 33F05

Nomenclature

Symbol	Description	Symbol	Description
ρ	Density of the medium	u, w	Displacement components
ρ_s	Density of the semiconductor	π, ψ	Two scalar functions
ρ_w	Density of the pore water	N	Carrier density
$T_\circ$	Absolute temperature	P	Pore water pressure
c_e	Specific heat of the medium	P_a	Acoustic pressure
c_s	Heat capacity of the semiconductor	λ, μ	Lamé's constants
c_w	Heat capacity of the pore water	b	Wave number
T	Temperature distribution	$n_\circ$	Porosity
D_E	Carrier diffusion coefficient	g	Gravity
d_n	Coefficients of electronic deformation	$H_\circ$	Magnetic field parameter
$\gamma = (3\lambda + 2\mu)\alpha_t$	Volume coefficient of the thermal expansion of volume	k_d	Coefficient of permeability
k	Thermal conductivity	E_g	Energy gap
α_t	Linear thermal expansion coefficient	τ	Lifetime
m	Volumetric heat capacity of the medium	$\tau_\circ$	Thermal memory
α_w	Linear thermal expansion coefficient of the pore water	μ_e	Magnetic permeability
$\delta_n = (3\lambda + 2\mu)d_n$	Deformation potential coefficient	σ_{ij}	Stress components
t	Time	ω	Angular frequency

1. Introduction

Wave propagation in porous semiconducting materials should be considered due to the necessity of studying the coupled interplay of mechanical, thermal, and electromagnetic fields that govern the material behavior. Despite the fact that pores in most semiconductors are usually either completely or partially closed, in practice, there may be such cases where some pores have air, humidity, or electrolyte inside; thus, fluid–solid coupling becomes physically meaningful for the study of wave propagation and energy transport. For the case of completely closed pores, it will follow that the model turns into the well-known model of the thermoelastic semiconductor, which validates the suggested approach. Photoelastic (thermo-optical) effects can be used to measure the stress and temperature distributions noninvasively, providing information about the energy redistribution within the medium under thermohydromechanical and electromagnetic effects. This approach enables the investigation of the problem in cases when fluid–solid coupling plays an important role and solves the problem of applicability of the proposed model for the case of porous semiconductors with partially filled or empty pores. Classical thermoelastic theories serve as the basis for this type of analysis, which

starts with the work of Biot in thermoelasticity and irreversible thermodynamics [1], followed by the generalized approach suggested by Lord and Shulman [2] and Green and Lindsay [3]. Wave propagation in saturated porous media has been studied due to its practical relevance in geophysics, microelectronics, and sensors. Tao et al. [4] analyzed wave characteristics in saturated thermoelastic porous media, and Othman and Singh [5] studied rotational effects in micropolar thermoelastic half-spaces. A mathematical model has been suggested for a semiconductor porous material under photothermoelastic excitation under initial stress by Raddadi et al. [6]. Coupled deterministic models have been created in order to simulate the interaction between mechanical, thermal, and diffusion processes. Salah et al. [7] examined magnetothermoelastic material with diffusion under hyperbolic, two-temperature photothermal waves, and Othman [8] discussed initial stress and gravity effects. Salah et al. [9] extended the analysis to rotating media with double porosity, and Othman and Hilal [10] investigated rotation and gravity effects on two-temperature materials. Abo-Dahab et al. [11] explored electromagnetic and photothermal wave propagation in rotating semiconductors. Stochastic effects have been incorporated to account for material inhomogeneities and random fluctuations. Sherief et al. [12] and Sakata et al. [13] investigated stochastic thermal shock problems and stochastic homogenization analysis, respectively. Meanwhile, Alenazi et al. [14] and Lotfy et al. [15] examined stochastic thermomechanical waves and stochastic photoelastothermodiffusion wave interactions in semiconductor materials, respectively. Salah et al. [16] studied nonlocal effects in rotating thermoelastic media with diffusion and double porosity, and Taha [17] analyzed white noise effects on stochastic thermohydromechanical photoelastic interactions. Lotfy et al. [18] developed stochastic photothermoelasticity models for excited semiconductor media. Photoelastic and photothermal techniques offer nondestructive means to monitor stress and temperature distributions. Salah et al. [19] investigated magnetic field and initial stress effects on rotating photothermal semiconductors. Lotfy [20,21] and Ailawalia [22] studied photothermal excitation, two-temperature waves, and ramp-type heating. Salah et al. [9] analyzed magnetothermoelastic responses in rotating double-porosity media, and Lotfy et al. [23,24] proposed models for ramp heating and nonlocal photothermoelastic interactions. Recent studies focused on multiphysics interactions combining rotation, magnetohydro effects, and multitemperature responses. Adel et al. [25] analyzed photoacoustic wave dynamics in magnetohydrosemiconductors, and Sheoran et al. [26] examined wave propagation in initially stressed rotating thermodiffusive media. In addition, efficient numerical schemes have been developed for related nonlinear and diffusion-type problems. Zhang et al. proposed a three-layer finite difference method [33] and a compact difference method [34] for the two-dimensional Kuramoto–Tsuzuki complex equation with strong nonlinear effects. Yang and Zhang [35] analyzed a new nonlinear finite volume scheme preserving the discrete maximum principle for the two-dimensional subdiffusion equation on distorted meshes, Ouyang and Zhang [36] constructed a hybrid Richardson method for the parabolic equation, and Liu and Zhang [37] developed an efficient GL-ADI general finite difference method for three-dimensional nonlocal diffusion equations with anisotropic diffusion coefficients.

The present study develops a deterministic coupled thermohydromechanical, photoelastic framework to investigate two-dimensional wave propagation in a fluid-saturated, porous, semiconducting half-space under the combined effects of gravity and magnetic fields. Unlike the previous stochastic model reported in [27], which did not account for gravitational or magnetic-field effects, the present formulation incorporates both effects into the governing equations, thereby extending the analysis to a broader range of coupled physical interactions. Especially noteworthy

is that the body force due to gravity gives rise to further coupling in longitudinal-transverse displacements, and the magnetic field accounts for electromagnetic interactions affecting the behavior of the material. Equations that include the theory of generalized thermoelasticity, hydromechanical coupling, photoelastic effects, and electromagnetic interactions are solved by employing the method of normal modes, where the numerical calculations are done by using Mathematica software. The impact of porosity, coupled-field parameters, gravity, and magnetic field intensity on the physical field profiles and magnitudes is examined. The analysis reveals an increased understanding of the interaction among thermal, mechanical, and plasma wave propagation through porous semiconductors, with possible implications for semiconductor-device engineering and photothermal sensors.

2. Formulation of the problem

The analysis presented in this paper considers an electromagnetothermoelastic half-space which is porous, semiconducting, and saturated with fluid. The solid medium has coupled behavior in the areas of thermoelasticity, hydromechanics, and photoelasticity, where the pore fluid is compressible. The system is assumed linear, isotropic, homogeneous, and undergoing small deformations. Let $(u, w)(x, z, t)$, $T(x, z, t)$, $N(x, z, t)$, $P(x, z, t)$, and $P_a(x, z, t)$ denote the displacement components, temperature change, carrier density, pore-fluid pressure, and photoacoustic pressure, respectively. The governing equations in the $x - z$ plane are formulated within the generalized photo-thermoelasticity framework, capturing the combined effects of material properties, coupled fields, and external forces on wave propagation in porous semiconductors. This framework builds on the coupled thermoelasticity theory of Biot [1] and the generalized theories of Lord and Shulman [2] and Green and Lindsay [3], together with the analyses of wave propagation in saturated thermoelastic porous media [4], rotating micropolar thermoelastic half-spaces [5], photothermoelastic porous semiconductors under initial stress [6], magnetothermoelastic semiconductors with diffusion [7], and the stochastic thermohydromechanical photoelastic model of poro-semiconductors [27]. The geometry of the problem is illustrated in Figure 1, which shows the fluid-saturated poro-semiconductor half-space, the x-axis along the direction of wave propagation and the z-axis normal to it, the gravity field g acting along the negative z-direction, and the applied magnetic field H. The figure also indicates the coupled thermal (T), carrier density (N), pore-water pressure (P), and photoacoustic pressure (P_a) fields that constitute the thermohydromechanical photoelastic interactions considered in this study.

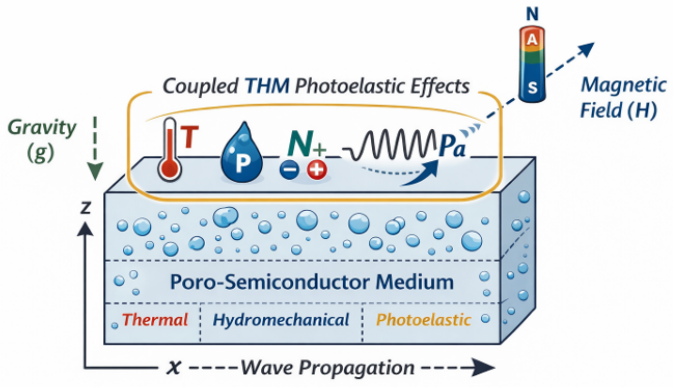


Figure 1. Problem geometry.

$$\left(\rho - \epsilon_0\mu_e^2H_0^2\right)\frac{\partial^2 u}{\partial t^2} = \left(\lambda + 2\mu + \mu_e H_\circ^2\right)\frac{\partial^2 u}{\partial x^2} + \left(\lambda + \mu + \mu_e H_\circ^2\right)\frac{\partial^2 w}{\partial x \partial z} + \mu\frac{\partial^2 u}{\partial z^2} - \rho g\frac{\partial w}{\partial x} - \frac{\partial P}{\partial x} - \gamma\frac{\partial T}{\partial x} - \delta_n\frac{\partial N}{\partial x}, \tag{1}$$

$$\left(\rho - \epsilon_0\mu_e^2H_0^2\right)\frac{\partial^2 w}{\partial t^2} = \left(\lambda + 2\mu + \mu_e H_\circ^2\right)\frac{\partial^2 w}{\partial z^2} + \left(\lambda + \mu + \mu_e H_\circ^2\right)\frac{\partial^2 u}{\partial x \partial z} + \mu\frac{\partial^2 w}{\partial x^2} + \rho g\frac{\partial u}{\partial x} - \frac{\partial P}{\partial z} - \gamma\frac{\partial T}{\partial z} - \delta_n\frac{\partial N}{\partial z}, \tag{2}$$

$$K\nabla^2 T - m\left(1 + \tau_{\mathrm{o}}\frac{\partial}{\partial t}\right)\frac{\partial T}{\partial t} - \gamma T_\circ\left(1 + \tau_{\mathrm{o}}\frac{\partial}{\partial t}\right)\left(\frac{\partial u}{\partial x} + \frac{\partial w}{\partial z}\right) + \frac{E_g}{\tau}N = 0, \tag{3}$$

$$\frac{\partial N}{\partial t} = D_E\nabla^2 N - \frac{1}{\tau}N + T, \tag{4}$$

$$b\left(\alpha_w\frac{\partial T}{\partial t} - \frac{\partial e}{\partial t}\right) - \rho_w\frac{\partial^2 e}{\partial t^2} + \nabla^2 P = 0, \tag{5}$$

$$\nabla^2 P_a - \frac{1}{c^2}\frac{\partial^2 P_a}{\partial t^2} - \partial\beta\frac{\partial T}{\partial t} = 0, \tag{6}$$

$$\sigma_{xx} = 2\mu\frac{\partial u}{\partial x} + \lambda e - \gamma T - P + (3\lambda + 2\mu)d_n N, \tag{7}$$

$$\sigma_{zz} = 2\mu\frac{\partial w}{\partial z} + \lambda e - \gamma T - P + (3\lambda + 2\mu)d_n N, \tag{8}$$

$$\sigma_{xz} = \mu\left(\frac{\partial u}{\partial z} + \frac{\partial w}{\partial x}\right), \tag{9}$$

$$e = \left(\frac{\partial u}{\partial x} + \frac{\partial w}{\partial z}\right), \tag{10}$$

where $m = n_{\mathrm{o}}\rho_w c_w + (1 - n_{\mathrm{o}})\rho_s c_s$, and $b = g\rho_w/k_d$.

The following nondimensional variables may prove useful in enhancing the transformation of the initial variables in the nondimensional case:

$$\left(x', z'\right) = c_\circ\xi(x, z), \quad \left(u', w'\right) = c_\circ\xi(u, w), \quad N' = \frac{\delta_n N}{\lambda + 2\mu}, \quad T' = \frac{\gamma T}{\lambda + 2\mu},$$
$$P' = \frac{P}{\lambda + 2\mu}, \quad P_a{}' = \frac{P_a}{P_\circ}\left(t', \tau', \tau_{\mathrm{o}}{}'\right) = c_\circ^2\xi\left(t, \tau, \tau_{\mathrm{o}}\right), \quad \sigma_{ij}' = \frac{\sigma_{ij}}{\mu}, \tag{11}$$
$$g' = \frac{Kg}{\rho c_e c_\circ^3}, \quad \xi = \frac{m}{K}, \quad c_\circ^2 = \frac{\lambda + 2\mu}{\rho}.$$

3. Solution of the problem

In this section, the Lamé's potentials approach is used together with the normal modes approach to enhance the accuracy of the solution without making any restrictive assumptions on the field variables. This can be done by the introduction of displacement potentials π and Ψ, which describe in a concise way the behavior of the displacement field. The relation between the displacements and the potential functions is given below:

$$u = \frac{\partial \pi}{\partial x} - \frac{\partial \Psi}{\partial z}, \qquad w = \frac{\partial \pi}{\partial z} + \frac{\partial \Psi}{\partial x}. \tag{12}$$

Incorporating the quantities in Eq (11) and the relations in Eq (12), we get the following equations:

$$\left(\varepsilon_{11}\nabla^2 - \varepsilon_{22}\frac{\partial^2}{\partial t^2} - \varepsilon_{33}\frac{\partial}{\partial z}\right)\pi - (P + T + N) = 0, \tag{13}$$

$$\left(\nabla^2 - B^2\frac{\partial^2}{\partial t^2} - \varepsilon_{44}\frac{\partial}{\partial z}\right)\psi = 0, \tag{14}$$

$$\left(\nabla^2 - \frac{\partial}{\partial t} - \tau_{\circ}\frac{\partial^2}{\partial t^2}\right)T - \varepsilon_8\nabla^2\left(\frac{\partial}{\partial t}\left(1 + \tau_{\circ}\frac{\partial}{\partial t}\right)\right)\pi + \varepsilon_7 N = 0, \tag{15}$$

$$\left(\nabla^2 - \varepsilon_1 - \varepsilon_2\frac{\partial}{\partial t}\right)N + \varepsilon_3 T = 0, \tag{16}$$

$$\nabla^2 P - \nabla^2\left(\varepsilon_4\frac{\partial}{\partial t} + \varepsilon_6\frac{\partial^2}{\partial t^2}\right)\pi + \varepsilon_5\frac{\partial T}{\partial t} = 0, \tag{17}$$

$$\left(\nabla^2 - \varepsilon_p\frac{\partial^2}{\partial t^2}\right)P_a - \eta_p\frac{\partial T}{\partial t} = 0, \tag{18}$$

$$\sigma_{xx} = \left(2\frac{\partial^2}{\partial x^2} + \frac{\lambda}{\mu}\nabla^2\right)\pi - \left(2\frac{\partial^2}{\partial x \partial z}\right)\psi - \beta^2(T + P - N), \tag{19}$$

$$\sigma_{zz} = \left(2\frac{\partial^2}{\partial z^2} + \frac{\lambda}{\mu}\nabla^2\right)\pi + \left(2\frac{\partial^2}{\partial x \partial z}\right)\psi - \beta^2(T + P - N), \tag{20}$$

$$\sigma_{xz} = \left(2\frac{\partial^2}{\partial x \partial z}\right)\pi + \left(\frac{\partial^2}{\partial x^2} - \frac{\partial^2}{\partial z^2}\right)\psi, \tag{21}$$

where

$$\nabla^2 = \frac{\partial^2}{\partial x^2} + \frac{\partial^2}{\partial z^2}, \quad \varepsilon_1 = \frac{1}{\tau D_E \xi}, \quad \varepsilon_2 = \frac{1}{D_E \xi}, \quad \varepsilon_3 = \frac{K\delta_n}{D_E c_{\circ}^2 \gamma \xi^2}, \quad \varepsilon_4 = \frac{b}{\xi(\lambda + 2\mu)},$$
$$\varepsilon_5 = \frac{b\alpha_w}{\gamma\xi}, \quad \eta_p = \partial\beta\frac{\rho c_{\circ}^2}{\gamma P_{\circ}\xi}, \quad \varepsilon_6 = \frac{\rho_w}{\rho}, \quad B^2 = \frac{\rho - \epsilon_0\mu_e^2 H_{\circ}^2}{\mu}, \quad \varepsilon_7 = \frac{\gamma E_g}{\tau m \delta_n},$$
$$\varepsilon_8 = \frac{\gamma^2 T_{\circ}}{m(\lambda + 2\mu)}, \quad \varepsilon_p = \frac{c_{\circ}^2}{c_s^2}, \quad \varepsilon_{11} = \frac{\lambda + 2\mu + \mu_e H_{\circ}^2}{\lambda + 2\mu}, \quad \varepsilon_{22} = 1 - \frac{\epsilon_0\mu_e^2 H_{\circ}^2}{\rho},$$
$$\varepsilon_{33} = \frac{\rho^2 c_e c_{\circ}^2 g}{m(\lambda + 2\mu)}, \quad \varepsilon_{44} = \frac{\rho^2 c_e c_{\circ}^2 g}{m\mu}, \quad \beta^2 = \frac{\lambda + 2\mu}{\mu}.$$

3.1. Normal mode technique

In this section, normal mode technique is employed, which has the advantage of finding the exact solutions without any assumed constraints on the field variables. Because the present study investigates wave propagation in a half-space medium unbounded in the z-direction and subjected to time-dependent disturbances, a normal mode analysis is adopted. The harmonic dependence in z and time represents traveling wave solutions and is physically justified for dynamic wave propagation in elastic and poroelastic media. This standard approach reduces the governing partial differential equations (PDEs) to a tractable set of ordinary differential equations (ODEs). Therefore, the physical variables under consideration can be decomposed in terms of normal modes [7,8] in the following form:

$$(\pi, \psi, T, N, P, P_a, \sigma_{ij})(x, z, t) = (\pi^*, \psi^*, T^*, N^*, P^*, {P_a}^*, {\sigma_{ij}}^*)(x)\, e^{(\omega t + ibz)}, \tag{22}$$

where the angular frequency, the imaginary number, and the wave number in the z-direction are denoted by ω, i, and b, respectively. Applying Eq (22) in Eqs (13)–(21), we have

$$\left(\varepsilon_{11}D^2 - \alpha_1\right)\pi^* - (P^* + T^* + N^*) = 0, \tag{23}$$

$$\left(D^2 - \alpha_2\right)\psi^* = 0, \tag{24}$$

$$\left(D^2 - \alpha_3\right)T^* - \alpha_4\left(D^2 - c^2\right)\pi^* + \varepsilon_7 N^* = 0, \tag{25}$$

$$\left(D^2 - \alpha_5\right)N^* + \varepsilon_3 T^* = 0, \tag{26}$$

$$\left(D^2 - c^2\right)P^* - \alpha_6\left(D^2 - c^2\right)\pi^* + \alpha_7 T^* = 0, \tag{27}$$

$$\left(D^2 - \alpha_8\right){P_a}^* - \alpha_9 T^* = 0, \tag{28}$$

$${\sigma_{xx}}^* = \left(\beta^2 D^2 - \alpha_{10}\right)\pi^* - \alpha_{11} D\psi^* - \beta^2(T^* + P^* - N^*), \tag{29}$$

$${\sigma_{zz}}^* = \left(\alpha_{12}D^2 - 3c^2\right)\pi^* - \alpha_{11} D\psi^* - \beta^2(T^* + P^* - N^*), \tag{30}$$

$${\sigma_{xz}}^* = \alpha_{11} D\pi^* - \left(D^2 - c^2\right)\psi^*, \tag{31}$$

where

$$\alpha_1 = \varepsilon_{11}c^2 + \varepsilon_{22}\omega^2 + ic\varepsilon_{33}, \quad \alpha_2 = c^2 + B^2\omega^2 + ic\varepsilon_{44}, \quad \alpha_3 = c^2 + \omega + \tau_o\omega^2,$$
$$\alpha_4 = \varepsilon_8(\omega + \tau_o\omega^2), \quad \alpha_5 = c^2 + \varepsilon_1 + \varepsilon_2\omega, \quad \alpha_6 = \varepsilon_4\omega + \varepsilon_6\omega^2, \quad \alpha_7 = \varepsilon_5\omega,$$
$$\alpha_8 = c^2 + \varepsilon_p\omega^2, \quad \alpha_9 = \eta_p\omega, \quad \alpha_{10} = \frac{\lambda}{\mu}c^2, \quad \alpha_{11} = 2ic, \quad \alpha_{12} = \frac{\lambda}{\mu}, \quad D = \frac{d}{dx}.$$

By solving Eqs (23) and (25)–(28), a tenth-order homogeneous differential equation is derived, given by

$$\left[D^{10} + A_{11}D^8 + A_{22}D^6 + A_{33}D^4 + A_{44}D^2 + A_{55}\right]\{\pi^*, T^*, N^*, P^*, {P_a}^*\} = 0. \tag{32}$$

The characteristic equation corresponding to Eq (32) is

$$\lambda^{10} + A_{11}\lambda^8 + A_{22}\lambda^6 + A_{33}\lambda^4 + A_{44}\lambda^2 + A_{55} = 0, \tag{33}$$

where

$$A_{11} = \frac{-\alpha_1 - \alpha_4 - \alpha_6 - c^2\varepsilon_{11} - \alpha_3\varepsilon_{11} - \alpha_5\varepsilon_{11} - \alpha_8\varepsilon_{11}}{\varepsilon_{11}},$$

$$\begin{aligned} A_{22} = \frac{1}{\varepsilon_{11}}\big[& c^2\alpha_1 + \alpha_1\alpha_3 + 2c^2\alpha_4 + \alpha_1\alpha_5 + \alpha_4\alpha_5 + c^2\alpha_6 + \alpha_3\alpha_6 + \alpha_5\alpha_6 + \alpha_4\alpha_7 + \alpha_1\alpha_8 \\ & + \alpha_4\alpha_8 + \alpha_6\alpha_8 + c^2\alpha_3\varepsilon_{11} + c^2\alpha_5\varepsilon_{11} + \alpha_3\alpha_5\varepsilon_{11} + c^2\alpha_8\varepsilon_{11} + \alpha_3\alpha_8\varepsilon_{11} \\ & + \alpha_5\alpha_8\varepsilon_{11} + \alpha_4\varepsilon_3 - \varepsilon_{11}\varepsilon_3\varepsilon_7\big], \end{aligned}$$

$$\begin{aligned} A_{33} = \frac{1}{\varepsilon_{11}}\big[& -c^2\alpha_1\alpha_3 - c^4\alpha_4 - c^2\alpha_1\alpha_5 - \alpha_1\alpha_3\alpha_5 - 2c^2\alpha_4\alpha_5 - c^2\alpha_3\alpha_6 - c^2\alpha_5\alpha_6 \\ & - \alpha_3\alpha_5\alpha_6 - c^2\alpha_4\alpha_7 - \alpha_4\alpha_5\alpha_7 - c^2\alpha_1\alpha_8 - \alpha_1\alpha_3\alpha_8 - 2c^2\alpha_4\alpha_8 - \alpha_1\alpha_5\alpha_8 \\ & - \alpha_4\alpha_5\alpha_8 - c^2\alpha_6\alpha_8 - \alpha_3\alpha_6\alpha_8 - \alpha_5\alpha_6\alpha_8 - \alpha_4\alpha_7\alpha_8 - c^2\alpha_3\alpha_5\varepsilon_{11} - c^2\alpha_3\alpha_8\varepsilon_{11} \\ & - c^2\alpha_5\alpha_8\varepsilon_{11} - \alpha_3\alpha_5\alpha_8\varepsilon_{11} - 2c^2\alpha_4\varepsilon_3 - \alpha_4\alpha_8\varepsilon_3 + \alpha_1\varepsilon_3\varepsilon_7 + \alpha_6\varepsilon_3\varepsilon_7 \\ & + c^2\varepsilon_{11}\varepsilon_3\varepsilon_7 + \alpha_8\varepsilon_{11}\varepsilon_3\varepsilon_7\big], \end{aligned}$$

$$\begin{aligned} A_{44} = \frac{1}{\varepsilon_{11}}\big[& c^2\alpha_1\alpha_3\alpha_5 + c^4\alpha_4\alpha_5 + c^2\alpha_3\alpha_5\alpha_6 + c^2\alpha_4\alpha_5\alpha_7 + c^2\alpha_1\alpha_3\alpha_8 + c^4\alpha_4\alpha_8 \\ & + c^2\alpha_1\alpha_5\alpha_8 + \alpha_1\alpha_3\alpha_5\alpha_8 + 2c^2\alpha_4\alpha_5\alpha_8 + c^2\alpha_3\alpha_6\alpha_8 + c^2\alpha_5\alpha_6\alpha_8 \\ & + \alpha_3\alpha_5\alpha_6\alpha_8 + c^2\alpha_4\alpha_7\alpha_8 + \alpha_4\alpha_5\alpha_7\alpha_8 + c^2\alpha_3\alpha_5\alpha_8\varepsilon_{11} + c^4\alpha_4\varepsilon_3 \\ & + 2c^2\alpha_4\alpha_8\varepsilon_3 - c^2\alpha_1\varepsilon_3\varepsilon_7 - c^2\alpha_6\varepsilon_3\varepsilon_7 - \alpha_1\alpha_8\varepsilon_3\varepsilon_7 - \alpha_6\alpha_8\varepsilon_3\varepsilon_7 \\ & - c^2\alpha_8\varepsilon_{11}\varepsilon_3\varepsilon_7\big], \end{aligned}$$

$$A_{55} = \frac{1}{\varepsilon_{11}}\left[-c^2\alpha_1\alpha_3\alpha_5\alpha_8 - c^4\alpha_4\alpha_5\alpha_8 - c^2\alpha_3\alpha_5\alpha_6\alpha_8 - c^2\alpha_4\alpha_5\alpha_7\alpha_8 - c^4\alpha_4\alpha_8\varepsilon_3 + c^2\alpha_1\alpha_8\varepsilon_3\varepsilon_7 + c^2\alpha_6\alpha_8\varepsilon_3\varepsilon_7\right],$$

and $\lambda_i, i = 1, 2, 3, 4, 5, 6, 7, 8, 9, 10$ are the roots of this equation.

The solutions of Eqs (23)–(31), satisfying the boundedness condition as $x \to \infty$, can be expressed as

$$\psi^* = A_6 e^{-\sqrt{\alpha_2}x}, \tag{34}$$

$$T^* = \sum_{i=1}^{5} A_i e^{-\lambda_i x}, \tag{35}$$

$$N^* = \sum_{i=1}^{5} H_{1i} A_i e^{-\lambda_i x}, \tag{36}$$

$$\pi^* = \sum_{i=1}^{5} H_{2i} A_i e^{-\lambda_i x}, \tag{37}$$

$$P^* = \sum_{i=1}^{5} H_{3i} A_i e^{-\lambda_i x}, \tag{38}$$

$$P_a{}^* = \sum_{i=1}^{5} H_{4i} A_i e^{-\lambda_i x}, \tag{39}$$

$$\sigma_{xx}{}^{*} = \sum_{i=1}^{5} H_{5i} A_i e^{-\lambda_i x} + \alpha_{11} \sqrt{\alpha_2} A_6, \tag{40}$$

$$\sigma_{xz}{}^{*} = \sum_{i=1}^{5} H_{6i} A_i e^{-\lambda_i x} - \left(\alpha_2 - c^2\right) A_6, \tag{41}$$

$$u^{*} = \sum_{i=1}^{5} \left(-\lambda_i H_{2i}\right) A_i e^{-\lambda_i x} - icA_6 e^{-\sqrt{\alpha_2} x}, \tag{42}$$

$$w^{*} = \sum_{i=1}^{5} \left(icH_{2i}\right) A_i e^{-\lambda_i x} - \sqrt{\alpha_2} A_6 e^{-\sqrt{\alpha_2} x}, \tag{43}$$

where

$$H_{1i} = \frac{\varepsilon_3}{\alpha_5 - \lambda_i^2}, \quad H_{2i} = \frac{(\lambda_i^2 - \alpha_3) + \varepsilon_7 H_{1i}}{\alpha_4(\lambda_i^2 - c^2)}, \quad H_{3i} = \frac{\alpha_6\left(\lambda_i^2 - c^2\right) H_{2i} - \alpha_7}{\lambda_i^2 - c^2}, \quad H_{4i} = \frac{\alpha_9}{\lambda_i^2 - \alpha_8},$$
$$H_{5i} = \left(\beta^2 \lambda_i^2 - \alpha_{10}\right) H_{2i} - \beta^2 (1 + H_{3i} - H_{1i}), \quad H_{6i} = -\alpha_{11} \lambda_i H_{2i}.$$

By substituting Eqs (34)–(43) into the normal-mode representation given in Eq (22), the dimensionless expressions for the physical quantities (π, Ψ, T, N, u, w, P, P_a, σ_{ij}) are obtained as

$$\psi(x, z, t) = A_6 e^{-\sqrt{\alpha_2} x} e^{(\omega t + ibz)}, \tag{44}$$

$$T(x, z, t) = \sum_{i=1}^{5} A_i e^{-\lambda_i x} e^{(\omega t + ibz)}, \tag{45}$$

$$N(x, z, t) = \sum_{i=1}^{5} H_{1i} A_i e^{-\lambda_i x} e^{(\omega t + ibz)}, \tag{46}$$

$$\pi(x, z, t) = \sum_{i=1}^{5} H_{2i} A_i e^{-\lambda_i x} e^{(\omega t + ibz)}, \tag{47}$$

$$P(x, z, t) = \sum_{i=1}^{5} H_{3i} A_i e^{-\lambda_i x} e^{(\omega t + ibz)}, \tag{48}$$

$$P_a(x, z, t) = \sum_{i=1}^{5} H_{4i} A_i e^{-\lambda_i x} e^{(\omega t + ibz)}, \tag{49}$$

$$\sigma_{xx}(x, z, t) = \left[\sum_{i=1}^{5} H_{5i} A_i e^{-\lambda_i x} + \alpha_{11} \sqrt{\alpha_2} A_6\right] e^{(\omega t + ibz)}, \tag{50}$$

$$\sigma_{xz}(x, z, t) = \left[\sum_{i=1}^{5} H_{6i} A_i e^{-\lambda_i x} - \left(\alpha_2 - c^2\right) A_6\right] e^{(\omega t + ibz)}, \tag{51}$$

$$u(x, z, t) = \left[\sum_{i=1}^{5} \left(-\lambda_i H_{2i}\right) A_i e^{-\lambda_i x} - icA_6 e^{-\sqrt{\alpha_2} x}\right] e^{(\omega t + ibz)}, \tag{52}$$

$$w(x, z, t) = \left[\sum_{i=1}^{5} \left(icH_{2i}\right) A_i e^{-\lambda_i x} - \sqrt{\alpha_2} A_6 e^{-\sqrt{\alpha_2} x}\right] e^{(\omega t + ibz)}. \tag{53}$$

4. Boundary conditions

Solving the governing equations necessitates the proper choice of boundary conditions on the plane $x = 0$, which describes the actual behavior of the fluid-saturated, porous semiconductor half-space subjected to gravitational and electromagnetic forces.

4.1. Photoacoustic pressure condition

The photoacoustic pressure at the surface, arising from thermoelastic and carrier-induced volumetric effects, is assumed to propagate freely into the surrounding medium:

$$P_a(0, z, t) = 0. \tag{54}$$

4.2. Thermal boundary condition

The surface temperature is prescribed to represent a thermal response under electromagnetic interactions, without any external laser source:

$$T(0, z, t) = T_0 e^{(\omega t + ibz)}, \tag{55}$$

where T_0 is a constant.

4.3. Pore-fluid boundary condition

Following Biot's poroelastic theory, the surface is assumed to have no hydraulic exchange with the environment, even in the presence of gravity:

$$P(0, z, t) = 0. \tag{56}$$

4.4. Carrier density boundary condition

At the surface, the carrier flux is balanced under applied electric and magnetic fields, ensuring charge conservation:

$$N(0, z, t) = N_0, \tag{57}$$

where N_0 is the equilibrium carrier concentration.

4.5. Mechanical boundary condition

The surface is considered traction-free, meaning that both normal and shear stresses vanish at $x = 0$. Gravity and electromagnetic body forces act within the medium but do not impose additional surface tractions:

$$\sigma_{xx}(0, z, t) = \sigma_{xz}(0, z, t) = 0. \tag{58}$$

By combining Eqs (54)–(58), a system of six equations for the constants is

obtained, A_1, A_2, A_3, A_4, A_5, and A_6, as follows:

$$\begin{pmatrix} H_{41} & H_{42} & H_{43} & H_{44} & H_{45} & 0 \\ 1 & 1 & 1 & 1 & 1 & 0 \\ H_{11} & H_{12} & H_{13} & H_{14} & H_{15} & 0 \\ H_{31} & H_{32} & H_{33} & H_{34} & H_{35} & 0 \\ H_{51} & H_{52} & H_{53} & H_{54} & H_{55} & R_M \\ H_{61} & H_{62} & H_{63} & H_{64} & H_{65} & R_N \end{pmatrix} \begin{pmatrix} A_1 \\ A_2 \\ A_3 \\ A_4 \\ A_5 \\ A_6 \end{pmatrix} = \begin{pmatrix} 0 \\ R_H \\ 0 \\ N_o \\ 0 \\ 0 \end{pmatrix}. \tag{59}$$

To determine the constants $A_i, i = 1, 2, 3, 4, 5, 6$, Cramer's method is applied to Eq (59), where $R_M = \alpha_{11}\sqrt{\alpha_2}$, $R_N = -\left(\alpha_2 - c^2\right)$, $R_H = \gamma T_0/(\lambda + 2\mu)$.

$$A_1 = \frac{\Delta A_1}{\Delta}, \quad A_2 = \frac{\Delta A_2}{\Delta}, \quad A_3 = \frac{\Delta A_3}{\Delta}, \quad A_4 = \frac{\Delta A_4}{\Delta}, \quad A_5 = \frac{\Delta A_5}{\Delta}, \quad A_6 = \frac{\Delta A_6}{\Delta}. \tag{60}$$

The constants $(A_1, \ldots, A_6)$ are determined using Cramer's rule, provided that the determinant of the coefficient matrix, Δ, is nonzero. If $\Delta = 0$, the coefficient matrix becomes singular, and Cramer's rule cannot be applied. This case may correspond to nonunique solutions or possible resonant conditions and requires a separate investigation.

5. Validation, stability analysis, and physical admissibility of the proposed model

The accuracy and physical reliability of the obtained analytical and computational solutions were carefully examined through several mathematical and physical validation procedures. Because the present formulation is based on the normal mode technique, the overall behavior of the coupled field variables is fundamentally controlled by the properties of the obtained roots of the auxiliary equation and the admissibility of the associated solutions. Accordingly, both boundedness conditions and stability requirements were analyzed to ensure the correctness of the proposed formulation. The first validation criterion was based on the physical boundedness of the solution in the semi-infinite domain. For a physically meaningful thermoelastic response, all field variables must remain finite and decay gradually as x $\to \infty$. This condition is satisfied when the selected roots of the auxiliary equation fulfil the admissibility requirement $\mathrm{Re}(\lambda_j) > 0$, which guarantees exponentially decaying solutions of the form $e^{-\lambda_j x}$. Consequently, only roots of the auxiliary equation possessing positive real parts were retained in the analytical construction of the solution, whereas roots leading to growing or unbounded responses were excluded. This selection criterion ensures spatial convergence of the temperature, normal stress, displacement component, carrier density, acoustic pressure, and water pressure within the medium. Similar admissibility conditions were adopted in related thermoelastic roots of the auxiliary equation formulations reported in the literature [25]. In addition to the boundedness requirement, the obtained analytical solution was verified through satisfaction of the imposed boundary conditions at the illuminated surface $x = 0$. The unknown constants $(A_1, \ldots, A_6)$ appearing in the general solution were evaluated such that all prescribed temperature, normal stress, acoustic pressure, water pressure, and carrier density boundary constraints were simultaneously satisfied. This procedure guaranteed consistency between the mathematical model and the underlying physical assumptions governing the isotropic semiconductor medium. The stability of the system was further assessed through examination of the qualitative behavior of the computed field distributions.

Stable solutions were characterized by smooth and continuously decaying spatial profiles without nonphysical divergence or irregular oscillatory growth. In contrast, unstable responses may arise when improper roots of the auxiliary equation are selected or when the admissibility conditions are violated. Roots of the auxiliary equation having negative real parts generate exponentially increasing solutions, leading to physically unacceptable behavior in the semi-infinite domain. Therefore, such roots were discarded during the roots of the auxiliary equation selection procedure. It is important to note that complex roots of the auxiliary equation may still produce physically acceptable solutions provided that their real parts remain positive. In such cases, the resulting fields exhibit attenuated oscillatory wave behavior, representing propagating thermoelastic waves accompanied by exponential spatial decay. This behavior reflects the combined influence of wave propagation inside the coupled isotropic medium. Furthermore, the influence of governing parameters such as time, permeability, electric field, magnetic field, and gravity field intensity was reflected directly through their effects on the eigenvalue spectrum. Variations in these parameters modify the characteristics of the coupled fields, thereby influencing the stability and localization behavior of the thermoelastic response. Appropriate parameter selection therefore plays an essential role in obtaining stable and physically admissible solutions. Additional validation was achieved through comparison with previously published limiting and related cases available in the literature, where good qualitative agreement was observed between the present results and earlier thermoelastic semiconductor models. This agreement confirms the mathematical consistency and computational reliability of the proposed isotropic photothermoelastic formulation. In the present investigation, a comprehensive analytical and numerical framework was developed to study the coupled thermophotoelastic–carrier interactions in an isotropic semiconductor medium under the influence of magnetic field, permeable electric field, and gravity field effects. The governing equations were transformed into a system of ordinary differential equations, allowing the application of the normal mode method to derive the complete general solution in terms of admissible curves. The obtained numerical results demonstrated that the coupled physical fields strongly depend on isotropy, magnetic field, permeable electric field, and gravity field. The normal stress, temperature, displacement, carrier density, acoustic pressure, and water pressure all exhibited decaying behavior away from the boundary surface, confirming the boundedness and stability of the proposed model. Moreover, the displacement fields displayed noticeable nonmonotonic characteristics, whereas the stress components showed strong sensitivity to isotropic, time, magnetic field, and gravity field effects. The spatiotemporal distributions further revealed that the dominant physical variations are concentrated near the illuminated boundary and attenuate progressively inside the medium. Photothermal influence introduced clear directional dependence into the physical response, whereas time, magnetic field, and gravity field effects significantly modified wave propagation and mechanisms. Overall, the present study demonstrates that the interaction between thermal effects, carrier transport, isotropic elasticity, magnetic field, gravity field parameter, and permeable electric field produces highly coupled and physically consistent responses. The obtained results provide useful theoretical insight for the analysis, design, and optimization of advanced semiconductor materials and engineering devices operating under coupled multiphysical environments.

6. Validity of the model

To validate the present formulation, a special case is first considered by neglecting the gravity

and magnetic field effects ($g = 0, H_{\mathrm{o}} = 0$). Under these assumptions, the governing equations reduce exactly to those presented by Alshalhoub et al. [27]. Figure 2 presents comparisons between the present results and the corresponding published results. An excellent agreement is observed for all physical quantities, confirming the correctness and reliability of the developed mathematical formulation and the numerical procedure. Moreover, the amplitudes of all physical quantities increase with increasing time, and the agreement between the present and published results becomes more pronounced with increasing distance, where the corresponding curves almost coincide within the interval ($2 \leq x \leq 3$). As a second limiting case, the hydromechanical pressure, photoacoustic pressure, gravity, and magnetic field effects are neglected ($P = 0$, $P_a = 0$, $g = 0$, $H_0 = 0$). Under these assumptions, the present formulation is reduced to a photothermoelastic semiconductor model comparable to those reported in [20,22,30], providing an additional theoretical verification of the proposed formulation. Furthermore, to satisfy the experimental validation requirement, the present model is further tuned to a simplified silicon laser-excitation case and compared qualitatively with the available experimental observations reported in [31,32]. The predicted thermoelastic response exhibits the same overall behavior as the experimentally observed response, demonstrating that the present formulation successfully reproduces the essential physical characteristics of laser-induced thermoelastic wave propagation in silicon. This qualitative agreement further confirms the validity, consistency, and applicability of the proposed model.

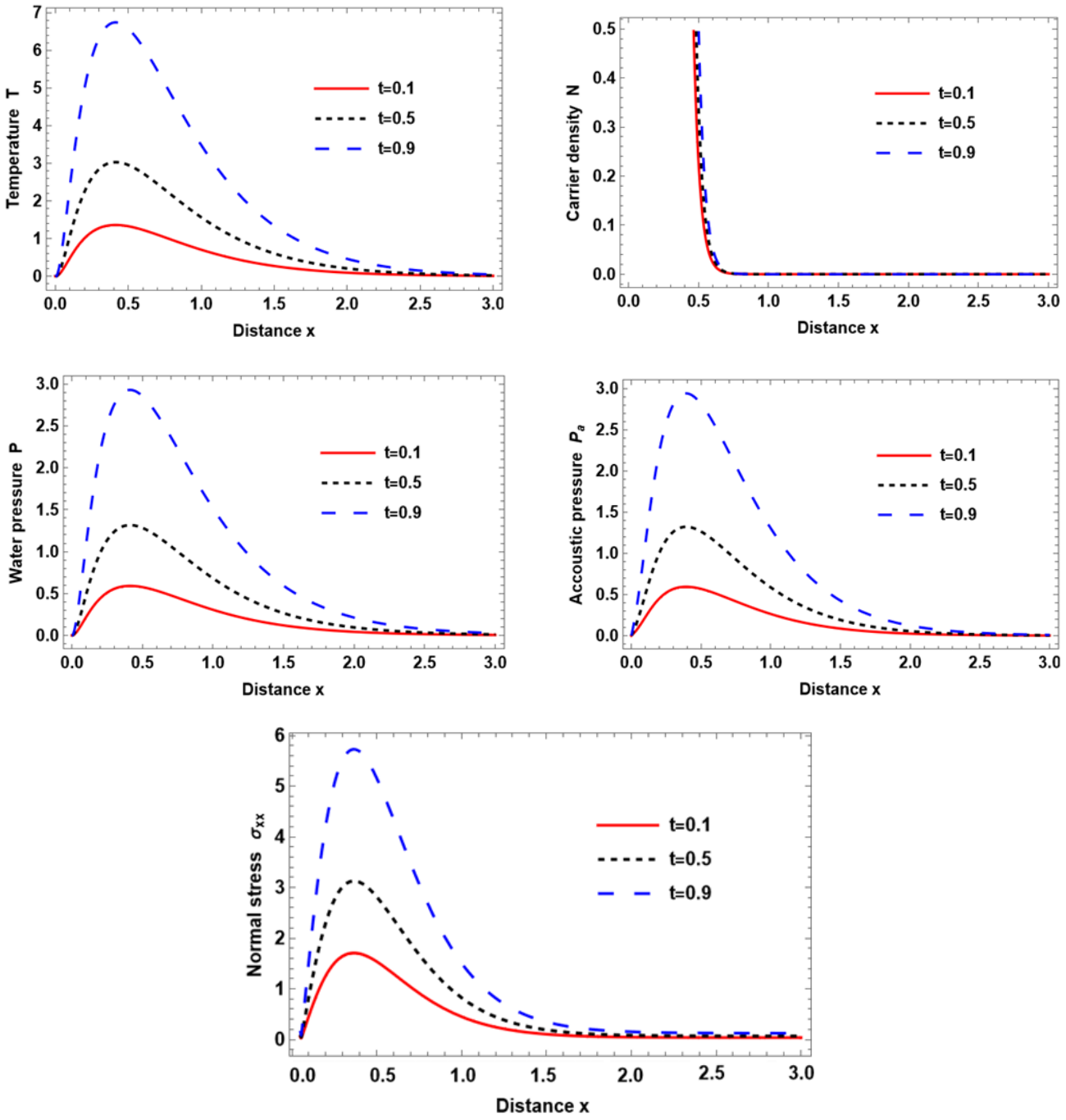


Figure 2. Validation of the present model through comparison with the published results in the absence of gravity field and magnetic field.

7. Numerical results and discussion

This section analyzes wave propagation in a fluid-saturated, porous, semiconducting medium, highlighting coupled thermoelastic, hydromechanical, and electromagnetic responses under gravity. Key physical fields including displacement, temperature, carrier density, pore-fluid pressure,

photoacoustic pressure, and stress are studied using numerical simulations with representative material properties (Table 1). Normal mode solutions are visualized in Mathematica, providing clear graphical insight into the dynamic interactions. These analyses reveal the complex interplay between thermohydromechanical and photoelastic effects in the medium [7,11,25].

Table 1. Material properties used in the numerical computations.

Unit	Symbol	Value	Unit	Symbol	Value
$N.m^{-2}$	λ	3.64×10^{10}	$m^2.s^{-1}$	d_n	-9×10^{-31}
$N.m^{-2}$	μ	5.46×10^{10}	$kg.m^{-3}$	ρ	2000
$kg.m^{-3}$	ρ_s	2300	cm^{-3}	N_o	9.65×10^9
K	T_o	800	$m^2.s^{-1}$	D_E	2.5×10^{-3}
Sec(s)	τ	5×10^{-5}	eV	E_g	1.11
K^{-1}	α_s	4.14×10^{-6}	N	P	100
$W.m^{-1}K^{-1}$	K	150	$Col^2.cl^{-1}.cm.s$	σ_o	9.36×10^5
$J.Kg^{-1}.K^{-1}$	C_e	695	$kg.m^{-3}$	ρ_w	1000
$m.s^{-1}$	k_d	10^{-8}	$H.m^{-1}$	μ_e	$4\pi \times 10^{-7}$
Sec(s)	τ_o	0.0002	$J.Kg^{-1}.K^{-1}$	C_s	6×10^2
K^{-1}	α_w	2×10^{-4}	$J.Kg^{-1}.K^{-1}$	C_w	4×10^3
$J.Kg^{-1}.K^{-1}$	C_e	695	m^{-3}	n_o	10^{20}
—	ω	2	—	c	2
$m.s^{-2}$	g	9.8	—	H_o	10^5

Figure 3 illustrates the variations of the temperature T, carrier density N, pore-water pressure P, acoustic pressure P_a, displacement u, and normal stress σ_{xx} with respect to the axial coordinate x for different values of time t. It is observed that the results indicate that all physical quantities evolve distinctly over time due to the coupled thermo–hydro–mechanical interactions. It is noted that the temperature, carrier density, pore-water pressure, acoustic pressure, displacement, and normal stress increase with time. Across the spatial domain, the temperature, pore-water pressure, acoustic pressure, and normal stress exhibit pronounced peaks for large values of axial displacement. The peak amplitudes increase with time, indicating that the transient response becomes more pronounced as time progresses, whereas the values away from the peaks gradually diminish. This behavior highlights the nonuniform spatial distribution of the physical fields and the time-dependent variation in wave amplitudes. Overall, these results demonstrate the significant influence of time on the evolution of the coupled physical quantities and the propagation of waves within the porous semiconducting medium. The observed behavior is in good qualitative agreement with the results reported by Alshalhoub et al. [27].

Figure 4 shows the variations of the temperature T, carrier density N, pore-water pressure P, acoustic pressure P_a, displacement u, and normal stress σ_{xx} with respect to the axial coordinate x for different values of electric permittivity ϵ_0. It is observed that the results reveal a nonuniform influence of the electric permittivity on the physical quantities. It is noticed that the carrier density, pore-water pressure, and normal stress increase with increasing electric permittivity, whereas the temperature, acoustic pressure, and displacement component decrease with increasing electric permittivity. This contrasting behavior can be physically explained by the redistribution of energy among the coupled thermal, mechanical, hydraulic, and carrier-diffusion fields. The electromagnetic interaction modifies

the motion and distribution of charge carriers, leading to changes in carrier concentration and consequently influencing the coupled hydraulic and mechanical responses. In particular, the increase in pore-water pressure and normal stress reflects the transmission of electromagnetic effects to the fluid and solid phases through their coupling mechanisms. Conversely, the reduction in temperature, acoustic pressure, and displacement indicates a weakening of the corresponding thermal and mechanical responses as the electromagnetic parameter increases. These interactions demonstrate that the electromagnetic parameter plays an important role in regulating the coupled behavior of the porous semiconductor.

Additionally, for the spatial profile of the variables, the values of the temperature, pore-water pressure, acoustic pressure, and normal stress have different maxima at various positions, followed by a gradual decay toward zero. This nonuniformity is due to the spatial propagation of coupled waves and the corresponding responses of interacting physical fields. Different positions of maxima of the values mean that each physical quantity has its own propagation property and energy distribution. In addition, the decay of the values with an increase in the distance is the result of the attenuation of wave disturbances and the corresponding dissipations and redistributions of energy in the medium. The change of the amplitude of the peak values with an electromagnetic parameter shows the effect of this parameter on the intensity and spatial distribution of the coupled effects. Finally, the slight difference between the three graphs shows that the spatial behavior of the studied phenomena is almost identical within the considered range of the electromagnetic parameter regardless of the changes in the values of physical quantities. This result is consistent with the findings obtained by Taha [17].

Figure 5 shows the variations of the temperature T, carrier density N, pore-water pressure P, acoustic pressure P_a, displacement u, and normal stress σ_{xx} with respect to the axial coordinate x for different values of magnetic field H_0. It is noted that the temperature, carrier density, pore-water pressure, and normal stress increase with increasing magnetic field strength, whereas the acoustic pressure and displacement component decrease with increasing magnetic field strength. The magnetic field suppresses mechanical and acoustic responses due to electromagnetic damping, whereas thermal and carrier-related quantities increase due to enhanced carrier confinement and modified heat transport. Pore-fluid and acoustic pressures reflect a balance between magnetic-induced stiffening and thermo–hydro–mechanical interactions. Overall, the results demonstrate that the magnetic field serves as an effective tuning parameter, highlighting the need for a fully coupled multiphysics formulation to capture the complex interactions in porous semiconducting media. Within the spatial domain, the physical quantities attain prominent peaks at varying positions, after which their values decline and gradually approach zero. The different peak positions reflect the distinct propagation characteristics of the coupled physical fields, and their gradual decay indicates wave attenuation with increasing distance. Moreover, increasing magnetic field intensity generally enhances the amplitudes of the physical quantities except for displacement and acoustic pressure, which exhibit an opposite trend. These variations demonstrate the influence of magnetic field intensity on both the magnitude and spatial distribution of the physical responses. These results are in good agreement with those reported by Salah et al. [7].

Figure 6 presents the variations of the temperature T, carrier density N, pore-water pressure P, acoustic pressure P_a, displacement u, and normal stress σ_{xx} with respect to the axial coordinate x for different values of gravity field g. It is observed that the temperature, carrier density, pore-water pressure, acoustic pressure, displacement component, and normal stress increase with increasing

gravitational acceleration. Thermal and carrier density fields are enhanced due to stronger mass transport and fluid–solid interactions, whereas pore-water pressure and acoustic response increase as the coupling between fluid motion and the solid matrix intensifies. The gravitational body force modifies the momentum balance and enhances the interaction between the solid skeleton and pore fluid, thereby affecting fluid pressure and deformation. In the same vein, both the displacement field and the stress field increase with an increase in gravity, indicating increased body forces and mechanical deformation, especially on the surface. This reveals that gravity is a global magnification factor that increases the coupling between the thermohydromechanical fields, hence increasing energy transfer among them. This implies that failure to consider gravity effects would greatly underestimate wave amplitudes.

The fields exhibit sharp peaks at different locations along the spatial domain and then gradually decay toward zero. The peak amplitudes increase with the considered parameter, showing that the system's dynamics strongly control both the magnitude and position of maximum responses. These localized peaks result from the interaction of coupled waves, and their gradual decay reflects spatial attenuation and energy redistribution among the physical fields.

Numerical simulations clearly show the interactions of time, electromagnetism, magnetism, and gravity on the physical fields in porous semiconductors. In terms of time evolution, all physical fields are affected. Electromagnetism and magnetism increase the carrier concentration, pore-fluid pressure, and stress but decrease displacement and acoustic pressure by virtue of Lorentz forces and electromagnetic damping. On one hand, electromagnetism influences the motion of charge carriers, but on the other hand, magnetism causes Lorentz forces due to the interplay between current densities and applied magnetic fields which, in turn, influence the mechanical behavior of the system. Gravity amplifies the effect of the coupled fields in relation to the coupling of thermal, diffusive, fluid, acoustic, and mechanical behaviors. These results qualitatively confirm earlier theoretical research, proving the accuracy of the model. The developed theory allows one to combine thermoelasticity, hydromechanics, electromagnetics, and photoelasticity into a single model, making it an effective tool for investigating the problems related to multiphysics wave propagation and material development. These results are in good agreement with previous publications [4,6,7,27].

Plasma recombination processes cause the carrier density, which represents plasma waves, to start with a positive value at the edge. Plasma waves, driven by optical-thermal energy and electromagnetic fields, peak abruptly at the surface, then retreat gradually according to an exponential decay curve as they travel into the semiconductor medium. This decay is associated with carrier diffusion and recombination, which reduce the carrier concentration as the disturbance propagates into the semiconductor. When the plasma waves approach the zero line, stability is achieved. According to experimental observations, the distribution decreases exponentially with distance from the surface until it reaches equilibrium at the zero line inside the semiconductor medium [28,29].

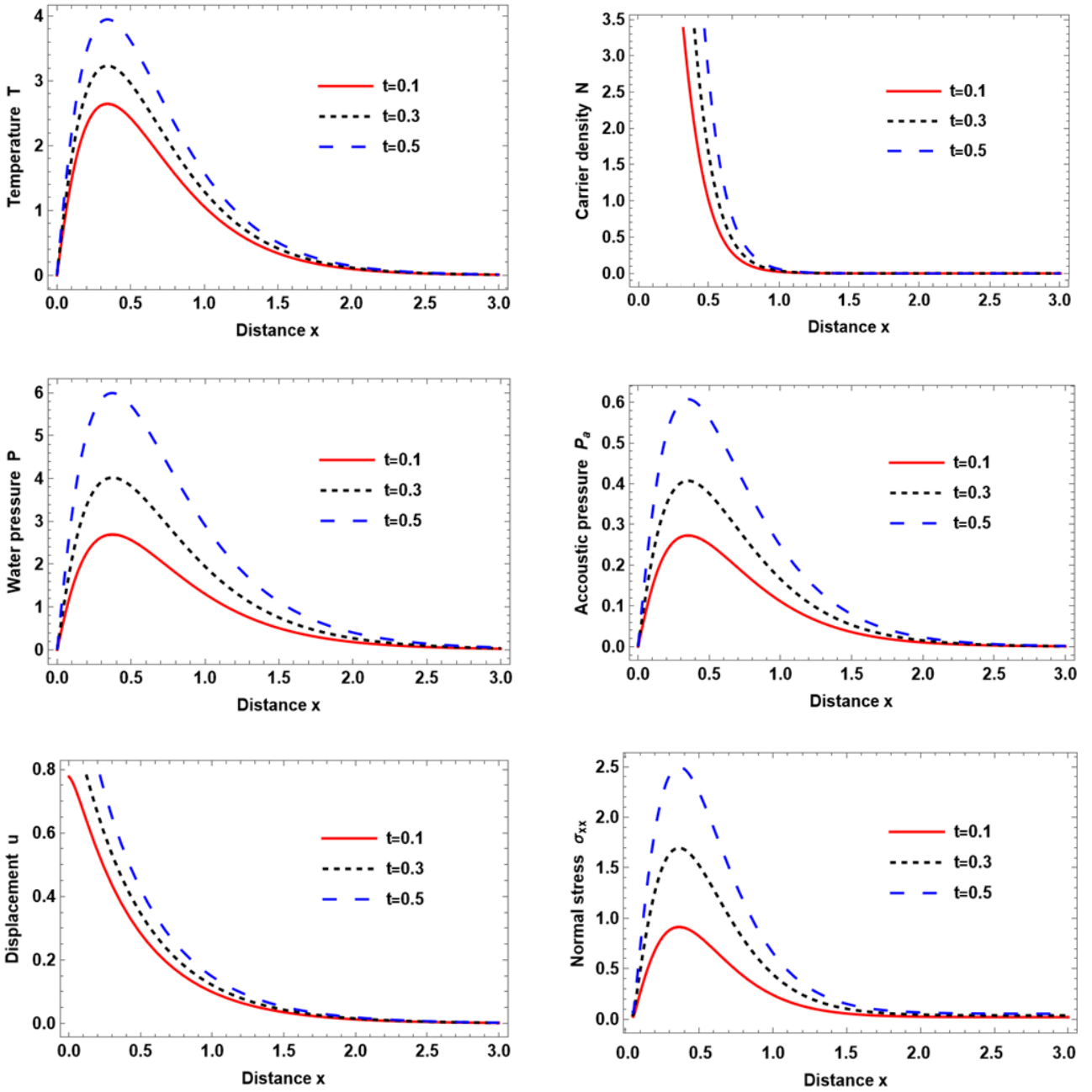


Figure 3. Time-dependent deterministic distributions of temperature, carrier density, pore pressure, acoustic pressure, displacement, and stress versus distance.

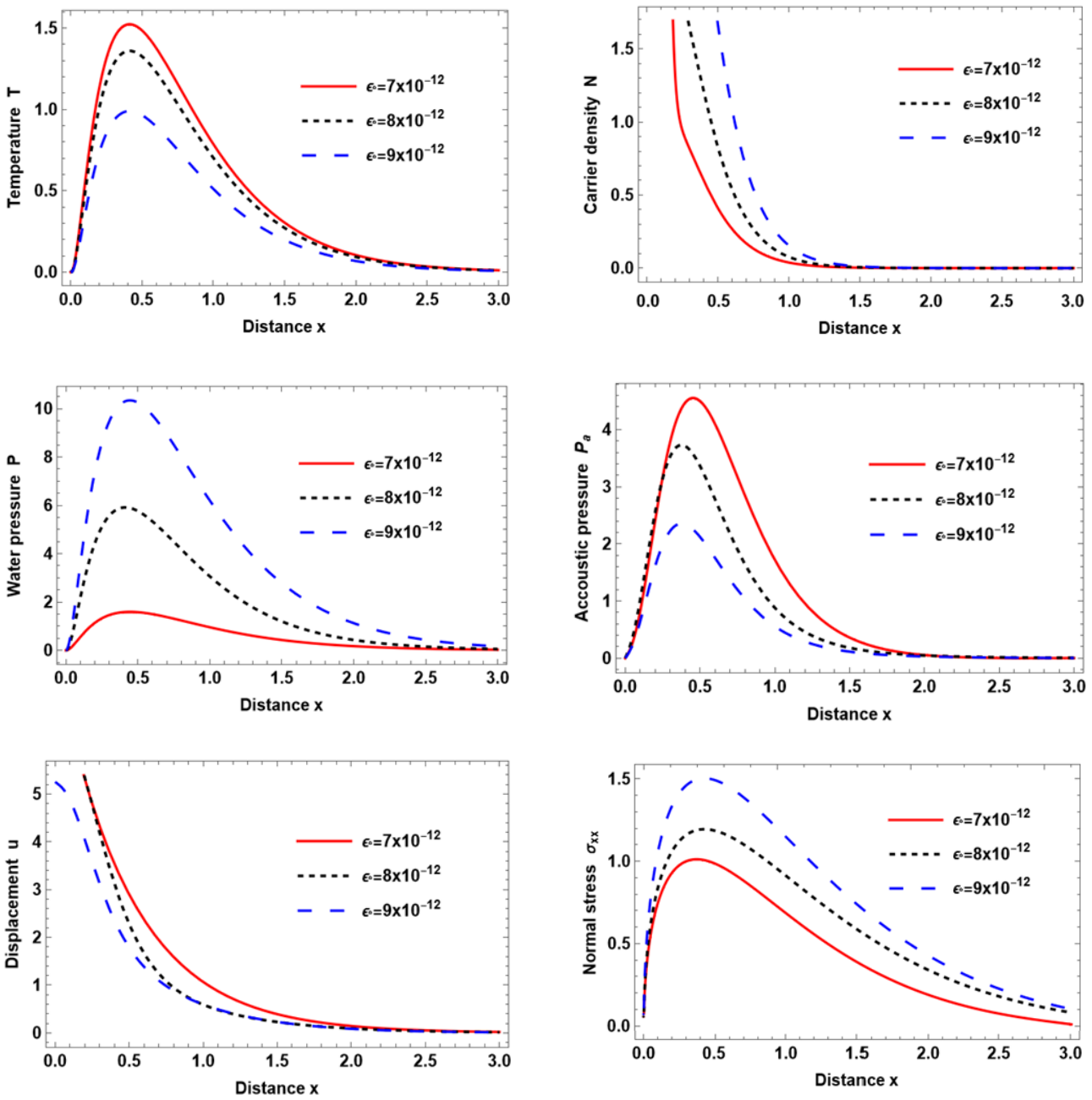


Figure 4. Temperature, carrier density, pore pressure, acoustic pressure displacement, and stress distributions with respect to distance due to the electric constant ϵ_0 in a deterministic manner.

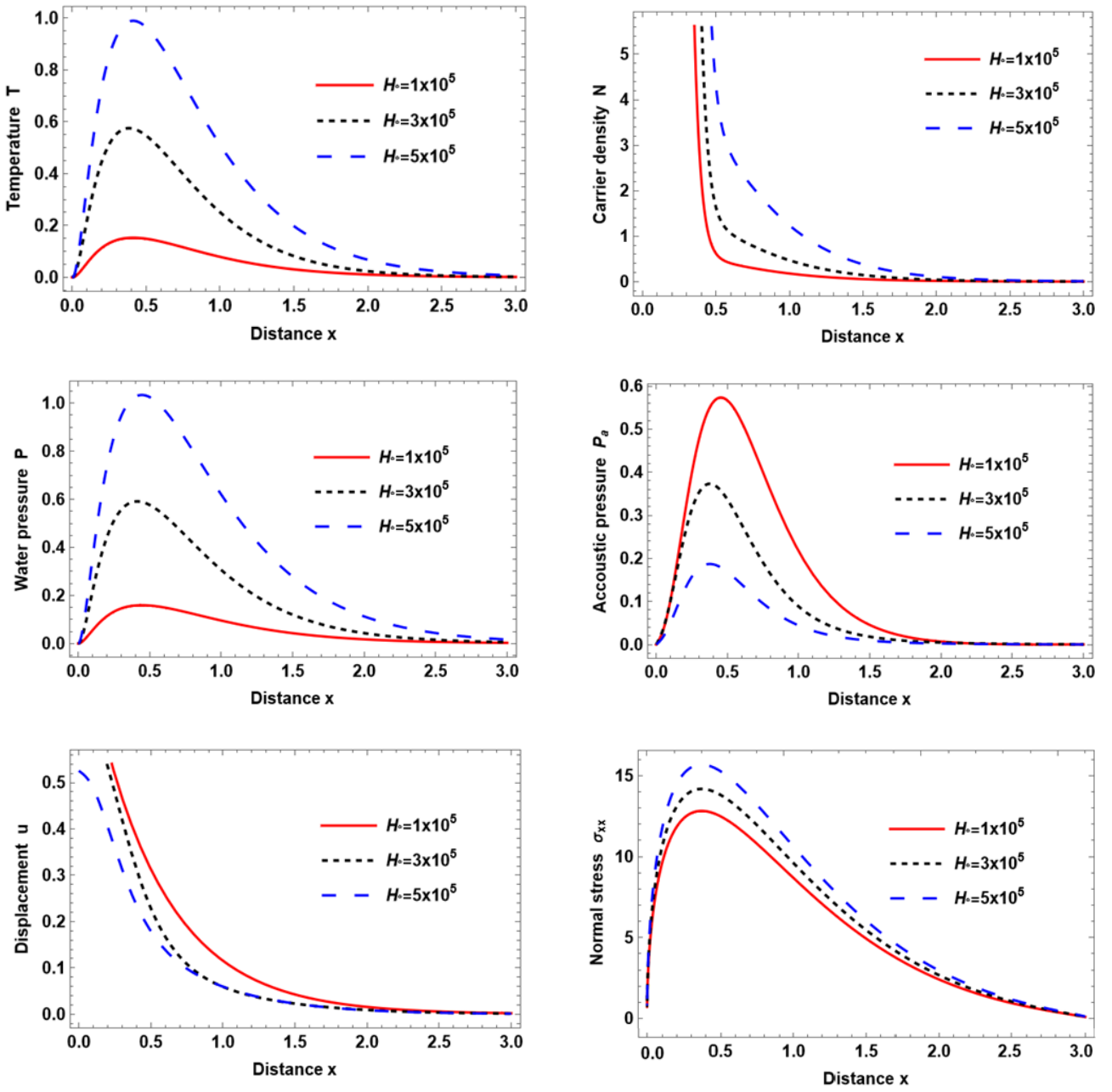


Figure 5. Deterministic distribution of temperature, carrier concentration, pore pressure, acoustic pressure displacement, and stress as a function of distance in the presence of a magnetic field.

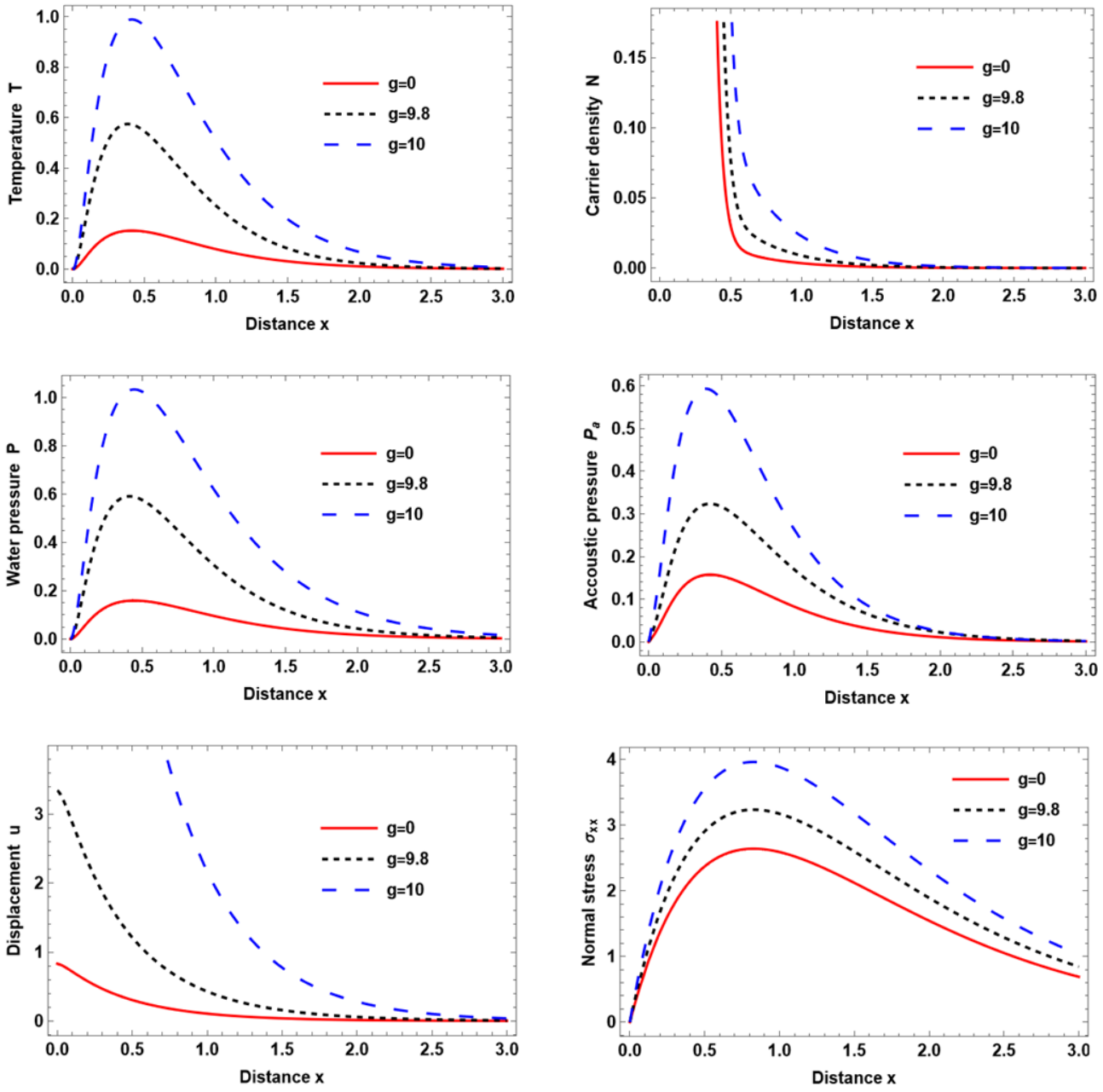


Figure 6. Deterministic distributions of temperature, carrier density, pore pressure, acoustic pressure displacement, and stress versus distance under the influence of gravity.

8. Conclusions

In this study, a deterministic coupled thermohydromechanical, photoelastic model was developed to investigate two-dimensional wave propagation in a fluid-saturated, porous semiconductor medium under the influence of gravity and electromagnetic fields. The governing equations were formulated by incorporating generalized thermoelasticity, hydromechanical coupling, photoelastic effects, and electromagnetic interactions. The resulting system was solved using the normal mode analysis

technique, and numerical computations were performed using Mathematica to examine the behavior of the coupled physical fields.

The main findings can be summarized as follows:

1. Time-dependent behavior: The temperature, carrier density, pore fluid pressure, acoustic pressure, displacement, and stress all increase with time, indicating the effects of time dependency on the propagation of waves.
2. Electromagnetic effect: There is a nonuniform variation of physical quantities due to the electromagnetic and magnetic field by increasing or decreasing their magnitude by electromagnetic coupling.
3. Gravitational effects: Gravity has a significant influence on the considered field variables, generally increasing their magnitudes and modifying the coupled thermohydromechanical response.
4. Material and coupling parameters: Changes in porosity and coupling parameters considerably affect the amplitudes and spatial distributions of the physical fields, highlighting the importance of material properties in determining wave behavior.
5. Boundary conditions: The obtained solutions satisfy the prescribed boundary conditions for pore-fluid pressure, acoustic pressure, and normal stress, ensuring the consistency of the mathematical formulation.

The current study can serve as an effective theoretical basis for the analysis of coupled wave propagation in poro-elastic semiconductors. The above-discussed model and the adopted methodology may be applied in different areas of thermodynamics, thermoelasticity, and materials science and could have practical implications in the development of semiconductors and photo-thermal sensors.

Author contributions

All authors contributed to the development of the study, analysis of the results, and preparation and revision of the manuscript. All authors have read and approved the final version of the manuscript for publication.

Use of Generative-AI tools declaration

The authors declare that they have not used Artificial Intelligence (AI) tools in the creation of this article.

Acknowledgements

The authors would like to express their sincere gratitude to King Faisal University for its generous support of this research.

Funding

This research was funded by the Deanship of Scientific Research, Vice Presidency for Graduate Studies and Scientific Research at King Faisal University [Grant No.KFU266515].

Data availability

The datasets used and/or analyzed during the current study are available from the corresponding author upon reasonable request.

Conflict of interest

The authors declare they have no conflicts of interest in this paper.

References

1. M. A. Biot, Thermoelasticity and irreversible thermodynamics, *J. Appl. Phys.*, **27** (1956), 240–253. https://doi.org/10.1063/1.1722351
2. H. W. Lord, Y. Shulman, A generalized dynamical theory of thermoelasticity, *J. Mech. Phys. Solids*, **15** (1967), 299–309. https://doi.org/10.1016/0022-5096(67)90024-5
3. A. E. Green, K. A. Lindsay, Thermoelasticity, *J. Elasticity*, **2** (1972), 1–7. https://doi.org/10.1007/BF00045689
4. H. Tao, G. Liu, K. Xie, R. Zheng, Y. Deng, Characteristics of wave propagation in the saturated thermoelastic porous medium, *Transport Porous Med.*, **103** (2014), 47–68. https://doi.org/10.1007/s11242-014-0287-6
5. M. I. A. Othman, B. Singh, The effect of rotation on generalized micropolar thermoelasticity for a half-space under five theories, *Int. J. Solids Struct.*, **44** (2007), 2748–2762. https://doi.org/10.1016/j.ijsolstr.2006.08.016
6. M. H. Raddadi, A. El-Bary, R. S. Tantawi, N. Anwer, K. Lotfy, A novel model of semiconductor porosity medium according to photo-thermoelasticity excitation with initial stress, *Crystals*, **12** (2022), 1603. https://doi.org/10.3390/cryst12111603
7. D. M. Salah, A. M. Abd-Alla, S. M. Abo-Dahab, Amnah M. Alharbi, M. A. Abdelhafez, Magneto-thermoelastic semiconductor medium with diffusion under the hyperbolic two-temperature photothermal waves, *Mech. Solids*, **59** (2024), 1774–1791. https://doi.org/10.1134/S0025654424603768
8. M. I. A. Othman, R. S. Tantawi, M. I. M. Hilal, Effect of initial stress and gravity field on micropolar thermoelastic solid with microtemperatures, *J. Theor. App. Mech.*, **54** (2016), 847–857. http://dx.doi.org/10.15632/jtam-pl.54.3.847
9. D. M. Salah, A. M. Abd-Alla, S. M. M. El-Kabeir, Magneto-thermoelastic response of a rotating medium with double porosity under initial stress, *Mech. Solids*, **60** (2025), 3303–3321. http://dx.doi.org/10.1134/S0025654425602010
10. M. I. A. Othman, M. I. M. Hilal, Rotation and gravitational field effect on two-temperature thermoelastic material with voids and temperature dependent properties type III, *J. Mech. Sci. Technol.*, **29** (2015), 3739–3746. http://dx.doi.org/10.1007/s12206-015-0820-8
11. S. M. Abo-Dahab, D. M. Salah, H. S. Gafel, A. M. Abd-Alla, M. A. Abdelhafez, Electromagnetic and heated pulse laser on wave propagation during electrons and holes excitation processes in a rotator semiconductor medium, *Sci. Rep.*, **15** (2025), 12877. http://dx.doi.org/10.1038/s41598-025-91584-x

12. H. H. Sherief, N. M. El-Maghraby, A. A. Allam, Stochastic thermal shock problem and study of wave propagation in the theory of generalized thermoelastic diffusion, *Math. Mech. Solids*, **22** (2017), 1767–1789. http://dx.doi.org/10.1177/1081286516644313
13. S. Sakata, F. Ashida, K. Fujiwara, A stochastic homogenization analysis for a thermoelastic problem of a unidirectional fiber-reinforced composite material with the homogenization theory, *J. Therm. Stresses*, **36** (2013), 405–425. http://dx.doi.org/10.1080/01495739.2013.770359
14. A. Alenazi, A. Ahmed, A. A. El-Bary, R. S. Tantawi, K. Lotfy, A stochastic thermo-mechanical waves with two-temperature theory for electro-magneto semiconductor medium, *Crystals*, **13** (2023), 82. http://dx.doi.org/10.3390/cryst13010082
15. K. Lotfy, A. El-Bary, E. Elidy, R. Tantawi, A. Ahmed, M. S. Mohamed, et al., A novel model of stochastic photo-elasto-thermodiffusion waves interaction in semiconductors, *Mech. Solids*, **59** (2024), 2301–2321. http://dx.doi.org/10.1134/S002565442460452X
16. D. M. Salah, A. M. Abd-Alla, S. M. M. El-Kabeir, Influence of nonlocal on a rotating thermoelastic medium with diffusion and double porosity, *Sci. Rep.*, **15** (2025), 15955. http://dx.doi.org/10.1038/s41598-025-97334-3
17. H. H. Taha, A. Ahmed, A. A. El-Bary, R. Tantawi, K. Lotfy, M. A. Fawzy, White noise effects on stochastic thermo-hydro-mechanical photoelastic interactions in poro-semiconductors, *J. Low Freq. Noise, V. A.*, **44** (2025), 2024–2048. http://dx.doi.org/10.1177/14613484251347811
18. K. Lotfy, A. Ahmed, A. El-Bary, A. El-Shekhipy, R. S. Tantawi, A novel stochastic photo-thermoelasticity model according to a diffusion interaction processes of excited semiconductor medium, *Eur. Phys. J. Plus*, **137** (2022), 972. http://dx.doi.org/10.1140/epjp/s13360-022-03185-6
19. D. M. Salah, A. M. Abd-Alla, S. M. Abo-Dahab, F. M. Alharbi, M. A. Abdelhafez, Magnetic field and initial stress on a rotating photothermal semiconductor medium with ramp type heating and internal heat source, *Sci. Rep.*, **14** (2024), 16456. http://dx.doi.org/10.1038/s41598-024-64485-8
20. K. Lotfy, A. A. El-Bary, A photothermal excitation for a semiconductor medium due to pulse heat flux and volumetric source of heat with thermal memory, *Waves Random Complex*, **31** (2021), 1303–1321. http://dx.doi.org/10.1080/17455030.2019.1662511
21. K. Lotfy, Photothermal waves for two temperatures with a semiconducting medium under using a dual-phase-lag model and hydrostatic initial stress, *Waves Random Complex*, **27** (2017), 482–501. http://dx.doi.org/10.1080/17455030.2016.1267416
22. P. Ailawalia, A. Kumar, Ramp type heating in a semiconductor medium under photothermal theory, *Silicon*, **12** (2020), 347–356. http://dx.doi.org/10.1007/s12633-019-00130-8
23. Kh. Lotfy, A. A. El-Bary, A. H. El-Sharif, Ramp-type heating microtemperature for a rotator semiconducting material during photo-excited processes with magnetic field, *Results Phys.*, **19** (2020), 103338. http://dx.doi.org/10.1016/j.rinp.2020.103338
24. K. Lotfy, A. Ahmed, A. El-Bary, R. S. Tantawi, A novel stochastic model of the photo-thermoelasticity theory of the non-local excited semiconductor medium, *Silicon*, **15** (2023), 437–450. http://dx.doi.org/10.1007/s12633-022-02021-x
25. M. Adel, S. El-Sapa, A. A. El-Bary, K. Lotfy, E. Can, Photoacoustic wave dynamics in magneto-hydro-semiconductor media with rotation and multi-temperature effects, *Case Stud. Therm. Eng.*, **72** (2025), 106432. http://dx.doi.org/10.1016/j.csite.2025.106432

26. D. Sheoran, R. Kumar, S. Kumar, K. K. Kalkal, Wave propagation in an initially stressed rotating thermo-diffusive medium with two-temperature and micro-concentrations, *Int. J. Numer. Method. H.*, **31** (2021), 1245–1267. http://dx.doi.org/10.1108/HFF-05-2020-0305
27. S. Alshalhoub, M. A. E. Nasr, K. Lotfy, I. S. Elshazly, A. A. El-Bary, R. Tantawi, et al., A stochastic photoacoustic thermo-hydro-mechanical photoelastic wave propagation investigation in poro-semiconductors materials, *Int. Commun. Heat Mass*, **169** (2025), 109951. http://dx.doi.org/10.1016/j.icheatmasstransfer.2025.109951
28. Y. Xiao, C. Shen, W. Zhang, Screening and prediction of metal-doped α-borophene monolayer for nitric oxide elimination, *Mater. Today Chem.*, **25** (2022), 100958. http://dx.doi.org/10.1016/j.mtchem.2022.100958
29. J. Liu, M. Han, R. Wang, S. Xu, X. Wang, Photothermal phenomenon: Extended ideas for thermophysical properties characterization, *J. Appl. Phys.*, **131** (2022), 065107. http://dx.doi.org/10.1063/5.0082014
30. M. I. A. Othman, R. S. Tantawi, E. E. M. Eraki, Propagation of the photothermal waves in a semiconducting medium under L-S theory, *J. Therm. Stresses*, **39** (2016), 1419–1427. http://dx.doi.org/10.1080/01495739.2016.1216063
31. X. Qi, C. S. Suh, Generalized thermo-elastodynamics for semiconductor material subject to ultrafast laser heating. Part I: Model description and validation, *Int. J. Heat Mass Tran.*, **53** (2010), 41–47. http://dx.doi.org/10.1016/j.ijheatmasstransfer.2009.10.010
32. D. K. Markushev, D. D. Markushev, S. M. Aleksić, D. S. Pantić, S. P. Galović, D. M. Todorović, et al., Experimental photoacoustic observation of the photogenerated excess carrier influence on the thermoelastic response of n-type silicon, *J. Appl. Phys.*, **128** (2020), 095103. http://dx.doi.org/10.1063/5.0015657
33. J. Zhang, X. Yang, S. Wang, A three-layer FDM for the Neumann initial-boundary value problem of 2D Kuramoto-Tsuzuki complex equation with strong nonlinear effects, *Commun. Nonlinear Sci.*, **152** (2026), 109255. http://dx.doi.org/10.1016/j.cnsns.2025.109255
34. J. Zhang, X. Yang, S. Wang, A compact difference method for the 2-D Kuramoto-Tsuzuki complex equation with Neumann boundary characterized by strong nonlinear effects, *Comput. Math. Appl.*, **203** (2026), 1–19. http://dx.doi.org/10.1016/j.camwa.2025.11.013
35. X. Yang, Z. Zhang, Analysis of a new NFV scheme preserving DMP for two-dimensional sub-diffusion equation on distorted meshes, *J. Sci. Comput.*, **99** (2024), 80. http://dx.doi.org/10.1007/s10915-024-02511-7
36. L. Ouyang, H. Zhang, Construction of a new hybrid Richardson method and its theoretical analysis for the parabolic equation, *Appl. Math. Lett.*, **182** (2026), 110043. http://dx.doi.org/10.1016/j.aml.2026.110043
37. J. Liu, H. Zhang, An efficient GL-ADI general finite difference method for three dimensional nonlocal diffusion equations with anisotropic diffusion coefficients, *Netw. Heterog. Media*, **21** (2026), 1709–1738. http://dx.doi.org/10.3934/nhm.2026064



AIMS Press

© 2026 the Author(s), licensee AIMS Press. This is an open access article distributed under the terms of the Creative Commons Attribution License (https://creativecommons.org/licenses/by/4.0)